Adjustable Event-Triggered Load Frequency Control of Power Systems Using Control Performance Standard-Based Fuzzy Logic

Xing-Chen Shangguan, *Student Member, IEEE,* Yong He, *Senior Member, IEEE,*
Chuan-Ke Zhang, *Senior Member, IEEE,* Lin Jiang, *Member, IEEE,* and Min Wu, *Fellow, IEEE.*

***Abstract*—This paper proposes a control performance standard (CPS)-based fuzzy event-triggered scheme for load frequency control (LFC) of power systems with a limited communication bandwidth. First, a CPS-based fuzzy LFC system is established to reduce the wear and tear of the generating unit equipment. Then, based on the Lyapunov stability theory, a stability criterion of LFC system is proposed to ensure the stable operation of the LFC system, which considers the threshold parameter of the event-triggered condition and the fuzzy gain in the fuzzy LFC system. Next, based on the stability criterion and the Guassian-type curve fitting method, a functional expression between the fuzzy gain and the threshold parameter is obtained. According to the expression, the threshold parameter is updated in real time with the change of fuzzy gain, so as to further save usage of the communication network bandwidth. Case studies based on a one-area power system and an IEEE 39-bus benchmark test system are undertaken. Simulation results show that the proposed scheme achieves three objectives: (i) to comply with the CPS1 and CPS2 in North American Electric Reliability Council; (ii) to reduce wear and tear of the generating unit equipment; and (iii) to save more communication network resources.**

***Index Terms*—Power systems, Load frequency control, Fuzzy control, Event-triggered control, Control performance standards 1 and 2, Limited communication bandwidth.**

I. Introduction

A. Research background

Load frequency control (LFC) plays a significant role in the frequency regulation of power systems [1]. The objective of LFC is to maintain the balance between load consumption and power generation to stay the frequency and tie-line power in the power system in an acceptable range [2, 3]. The feedback signals from the LFC center are used to maneuver the turbine governor setpoints of the generators so that the generated power follows the load fluctuations [4]. However, continuously tracking load fluctuations definitely causes wear and tear on generating unit equipment, shortens their lifetime, and might require replacements of these equipment, which can be very costly. In particular, restructuring of the electricity industry has forced vertically integrated utilities to split into independent and specialized companies, including generation, transmission, and distribution companies [5, 6]. New participants have emerged to compete in the generation business and to provide ancillary frequency regulation service using the LFC scheme. To benefit fully from this environment, market participants have to minimize their operating and maintenance costs associated with the maneuvering of the generating unit [7]. Therefore, reducing the wear and tear on the generating unit equipment is the expectation of future LFC scheme design.

On the other hand, with the increasing deployment of restructuring of the electricity industry, dispersed renewable energy sources and demand side responses, an efficient modern power system is suggested to use open communication networks to support these distributed devices [8, 9]. Modern power systems are evolving towards a new generation of smart grids, where the increasing deployment of phase measurement units and smart meters leads to a substantial increase in measurement/control signals in the open communication network [10, 11]. Concerning the large-scale deployment of these information technology infrastructures, tremendous data exchange would rapidly make the network load imbalanced and exhaust the network resources [12]. Power network operators have to face communication bottlenecks, leading to unreliable operations of power systems [13]. Constant signal transmission in LFC of power systems will waste many communication resources. Especially in bandwidth-limited networks, constant signal transmission will likely cause communication congestion, which can cause time delays and packet losses that degrade the control performance and even threaten the stability of the LFC system [14]. As reported in [15], the communication between generation units has bandwidth constraints in the practical LFC process. Therefore, it is desirable to design an effective LFC scheme that can save communication network bandwidth.

B. Literature review

Much attention has been paid to reducing wear and tear in LFC systems. The main method is to adjust the controller gains in the LFC scheme based on the North American Electrical Reliability Council (NERC)'s control performance standards (CPSs) instead of the asymptotic stability condition. Based on the frequency regulation requirements of the NERC, the frequency and tie-lie power only need to comply with CPS1 and CPS2 [16]. The standards require the frequency and tie-lie power to fluctuate within a certain range, which relaxes the requirements on LFC design. Fuzzy control systems have wide

This work was supported in part by the National Natural Science Foundation of China under Grants 62022074, 61973284 and 61873347, by the Hubei Provincial Natural Science Foundation of China under Grants 2019CFA040, by the 111 project under Grant B17040, and by the Fundamental Research Funds for National Universities, China University of Geosciences (Wuhan). *(Corresponding author: Yong He)*

X.C. Shangguan, Y. He, C.K. Zhang and M. Wu are with the School of Automation, China University of Geosciences, Wuhan 430074, China, with Hubei Key Laboratory of Advanced Control and Intelligent Automation for Complex Systems, Wuhan 430074, China, and also with Engineering Research Center of Intelligent Technology for Geo-Exploration, Ministry of Education, Wuhan 430074, China. (email: star@cug.edu.cn; heyong08@cug.edu.cn; ckzhang@cug.edu.cn; wumin@cug.edu.cn)

L. Jiang is with Department of Electrical Engineering and Electronics, University of Liverpool, Liverpool L69 3GJ, United Kingdom. (e-mail:ljiang@liv.ac.uk)

applications in telerobots of space medicine [17], cognitive infocommunications [18], tower crane systems [19] and power systems [20, 21]. Especially in power systems, fuzzy control as an intelligent control method for the design of smart grids provides much support [22, 23]. The regulation mechanism of the fuzzy control system can meet the requirements of CPS1 and CPS2 [24, 25]. Some fuzzy-based fuzzy LFC schemes have been proposed. Feliachi et al. presented a CPS-compliant fuzzy logic rule-based LFC scheme [7], while Pappachen et al. introduced a CPS-oriented adaptive neuro-fuzzy interface system controller for LFC of multi-area deregulated power systems [26]. Additionally, Belkacemi et al. [27] proposed an online immune-reinforcement-learning-based LFC scheme for a four-area power system in the presence of renewable-energy resources. In these researches, the CPSs are set as the inputs of the fuzzy control system or the online immune-reinforcement-learning system, and the integral controller gains in the LFC scheme are automatically tuned following the inputs of CPSs. The controller gains are reduced to diminish the high-frequency movement of the speed governor's equipment when the control area has high compliance with NERC standards.

An event-triggered (ET) communication scheme performs well in reducing the communication network burden [28, 29] and has been widely used in LFC systems. Wen et al. [30] presented an H_∞ ET LFC scheme for power systems to reduce the transmission amount of measurement/control signals while preserving the desired H_∞ robustness performance. Many scholars have done much work to improve the ET LFC scheme to further reduce the communication burden. For example, adaptive ET LFC schemes were developed in [31] and [32], where the threshold parameters can be adaptively adjusted to save more communication network resources. A switching-based ET LFC scheme was presented in [33], where the amount of sent measurement is reduced by switching between periodic sampling and continuous ET. Additionally, inspired by the use of CPSs to reduce controller parameters in [7], Ref. [34] proposed a decentralized CPS-oriented ET LFC scheme, where the selection constraints of the threshold parameter are relaxed compared with the previous research in [31]. The selection of a large threshold parameter in the scheme lowers the triggering frequency to further reduce the unnecessary transmission of measurement/control signals.

C. Motivations

Based on the above literature review, there are still some deficiencies. First, as stated in Ref. [39, 40], the practical LFC system is a sampled-data control system, where the update cycle of control signal is 2-4 s. The CPS-based fuzzy LFC schemes in [26, 27] did not consider the inherent update cycle of 2-4 s in the LFC system, and the schemes may not be effective due to the impact of the large update cycle of control signal. Additionally, although the proposed CPS-based fuzzy LFC scheme in [26, 27] reduced the wear and tear, it used the continuous transmission of measurement/control signals without taking into account the cost of network resources in an open communication network, which will aggravate the problems of transmission delays and packet losses, and may degrade the control performance. This is the first motivation. Second, to save communication network bandwidth, Shangguan et al. [34] employed CPSs to adjust the threshold parameters of ET condition, where only the individual measurement was used to change the selection of threshold parameters to meet the CPS requirements. However, the CPS is actually a statistical average standard. Therefore, the statistical properties in CPS are not used in Ref. [34]. Moreover, choosing a large threshold parameter in the literature may lead to LFC system instability. This is the second motivation. Finally, the existing research only focuses on reducing wear and tear [26, 27] or on saving communication network resources [31, 34]. To our knowledge, until now, there has been no research that considers both reducing wear and tear and lowering the usage of communication network resources to design LFC schemes. This is the third motivation.

D. Contributions

Based on the above discussions, this study proposes a CPS-based fuzzy event-triggered (FET) scheme for LFC of power systems with a limited communication bandwidth. An ET LFC model, which takes into account the sampling characteristics and time delay, is first established to reduce unnecessary measurement/control signal transmission. Next, a CPS-based fuzzy control system is designed to reduce wear and tear. Following the input of the compliance factor of CPS1, the fuzzy control system adaptively outputs the fuzzy gain to adjust the area control error (ACE) of the LFC system. Then, a stability criterion, considering the threshold parameter and the fuzzy gain, is derived to ensure the stability of the proposed control scheme based on the Lyapunov stability theory. The Guassian-type curve fitting method is employed to develop a function expression of the threshold parameter and the fuzzy gain under the stability criterion. Based on the function expression, the threshold parameter in the event-triggered scheme can be quickly solved and obtained under a dynamic fuzzy gain. The dynamic and adjustable threshold parameter is used to update the event-triggered condition to further lower the unnecessary signal transmission. The proposed control scheme achieves three objectives: (i) to comply with the NERC's CPS1 and CPS2; (ii) to reduce the wear and tear on generating unit equipment; and (iii) to lower unnecessary measurement/control signal transmission to save communication network resources. The effectiveness and advantages of the proposed control scheme are validated based on simulation tests of a one-area power system and an IEEE 39-bus benchmark test system. In summary, the main contributions are as follows.

(1) Different from the CPS-oriented ET LFC scheme in [34] and the CPS-based fuzzy LFC in [26], the proposed scheme achieves both reduced wear and tear and less unnecessary signal transmission in LFC systems while ensuring that the systems tend to just meet the NERC's CPS1 and CPS2.

(2) The stability of the LFC system with the proposed scheme is guaranteed. Different from the control scheme in [34], the adjustable threshold parameter of the event-triggered condition in the proposed control scheme is obtained through the stability condition of the LFC system, and

the statistical properties in CPS are used to improve the selection of the threshold parameter.

(3) The curve fitting method is used to find the function expression of the threshold parameter, the controller gain and the fuzzy gain. The threshold parameter is calculated based on the function expression to achieve real-time and fast updating of the event-triggered condition when the fuzzy gain and the controller gain are given.

(4) When the control area has high compliance with CPSs, a smaller fuzzy gain is generated via the fuzzy control scheme, and a larger threshold parameter is obtained based on the function expression. The reduction of the wear and tear and the decrease of the signal transmission are carried out in the same direction, and there is no need to compromise between them.

The remainder of this paper is organized as follows. Section II presents the ETLFC model. Section III proposes the CPS-based fuzzy-event-triggered LFC scheme. Section IV is the case studies to validate the effectiveness of the proposed control scheme. Conclusions are presented in Section V.

II. ET LFC MODEL

In this subsection, a dynamic model of ET LFC of power systems is introduced. This model considers the sampling and time delay in an open communication network.

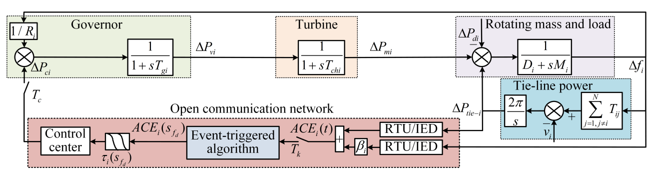

Fig. 1. ET LFC structure of i^{th} area of a multi-area power system.

A multi-area power system comprises N control areas that are interconnected by tie-lines. For every subarea i, assume that the generator in each control area is equipped with non-reheat turbine, and the similar linearized model is presented in Fig. 1, which includes the governor, the turbine, the rotating mass and load, the tie-line power, and the communication channel, where ΔP_{ci}, ΔP_{vi}, ΔP_{mi}, ΔP_{di}, Δf_i and ΔP_{tie-i} denote the control input, the valve position deviation, the generator mechanical output deviation, the load deviation, the frequency deviation and the tie-line power exchange deviation of the i^{th} area of the power system, respectively; β_i, R_i, M_i, D_i, T_{chi}, and T_{gi} are the frequency bias factor, the speed drop, moments of inertia of the generator, damping coefficient of the generator, time constant of the turbine, and time constant of the governor of the i^{th} area of the power system, respectively; T_{ij} is the tie-line synchronizing coefficient between area i and area j, and $v_i = \sum_{j=1,j\neq i}^{N} T_{ij}\Delta f_j$; ACE_i represents the area control error (ACE) of the i^{th} area and is the linear combination of Δf_i and ΔP_{tie-i}, i.e., $ACE_i = \beta_i \Delta f_i + \Delta P_{tie-i}$.

For the large-scale power system, the decentralized control strategy is suggested to be applied, as stated in [41]. The interactions between different areas, v_i, are treated as disturbances for each area. This means that every control area is independent and has its own LFC center to maintain the balance of generation and load. Then, define $\tilde{x}_i = [\Delta f_i, \Delta P_{tie-i}, \Delta P_{mi}, \Delta P_{vi}]^T$, $\tilde{y}_i = ACE_i$, and $\tilde{\omega}_i = [\Delta P_{di}, v_i]^T$. One can obtain the following LFC state-space model of the i^{th} area of the power system

$$\begin{cases} \dot{\tilde{x}}_i(t) = \tilde{A}_i \tilde{x}_i(t) + \tilde{B}_i \tilde{u}_i(t) + \tilde{F}_i \omega_i(t) \\ \tilde{y}_i(t) = \tilde{C}_i \tilde{x}_i(t) \end{cases} \tag{1}$$

where

$$(\tilde{A}_i)_{4\times4} = \begin{bmatrix} -\frac{D_i}{M_i} & -\frac{1}{M_i} & \frac{1}{M_i} & 0 \\ 2\pi\sum_{j=1,j\neq i}^{N} T_{ij} & 0 & 0 & 0 \\ 0 & 0 & -\frac{1}{T_{chi}} & \frac{1}{T_{chi}} \\ -\frac{1}{R_i T_{gi}} & 0 & 0 & -\frac{1}{T_{gi}} \end{bmatrix},$$

$$(\tilde{B}_i)_{4\times1} = \begin{bmatrix} 0 & 0 & 0 & \frac{1}{T_{gi}} \end{bmatrix}, (\tilde{C}_i)_{1\times4} = [\,\beta_i \;\; 1 \;\; 0 \;\; 0\,],$$

$$(\tilde{F}_i)_{4\times2} = \begin{bmatrix} -\frac{1}{M_i} & 0 & 0 & 0 \\ 0 & -2\pi & 0 & 0 \end{bmatrix}^T.$$

Choose the following integral-type controller

$$\tilde{u}_i(t) = -K_{I,i} \int ACE_i(t)dt \tag{2}$$

where $K_{I,i}$ is the integral gain.

Note that the measured $ACE_i(t)$ cannot be directly used due to the sampling of measurements, the ET scheme, and the time delay in the open communication network. As shown in Fig. 1, remote terminal units (RTUs) or intelligent electronic devices (IEDs) in an SCADA system are used for acquisition of the measurements (Δf_i and ΔP_{tie-i}). These measurements are then sent out at a time interval T_k. Since the power commands sent to generation units are updated at a time interval T_c within $[2, 4]$ s, the T_k is expected to have a larger value, that is preferably not less than the update interval T_c of control signals. To simplify the modeling and analysis, we assume that

(1) T_k is equal to T_c.

(2) The transmission instants s_k $(k = 1, 2, 3, \cdots)$ are synchronized among the RTUs or IEDs in different control areas. The sequence of $\{s_k\}$ is strictly increasing and goes to infinity as k increases. There exist two positive scalars $h_1 < h_2$ such that the difference between two successive sampling instants $T_k = s_{k+1} - s_k$ satisfies

$$0 < h_1 \leq T_k \leq h_2, \forall k \geq 0. \tag{3}$$

(3) The delays, including network-induced and fault-induced delays, are combined as one single delay $\tau_i(t)$, which is uncertain and time-varying with lower bound τ_m and upper bound τ_M and satisfies

$$0 \leq \tau_m \leq \tau_i(t) \leq \tau_M, |\dot{\tau}_i(t)| \leq \mu < 1. \tag{4}$$

where μ is the upper bound of the derivative of the time delay. In particular, if $\dot{\tau}_i(t) = 0$, then $\tau_i(t)$ is constant and $\tau_m = \tau_M$.

(4) The multiple delays $\tau_i(t)$ with $i = 1, 2, ..., N$ are all equal and considered as a single delay $\tau(t)$.

Then, the attainable $ACE_i(t)$ at the LFC center can be written as follows:

$$ACE_i(t) = ACE_i(s_k), t \in [s_k + \tau(s_k), s_{k+1} + \tau(s_{k+1})) \tag{5}$$

Denoting $t_k = s_k + \tau(s_k)$ as the updating instants of the control input $u_i(t)$, for $t \in [t_k, t_{k+1})$, the integral-type controller can be rewritten as

$$\tilde{u}_i(t) = \tilde{u}_i(s_k) = -K_{I,i} \int ACE_i(s_k)dt. \tag{6}$$

Define $x_i(t) = [\tilde{x}_i^T(t) \int \tilde{y}_i^T(t)]^T$ and $y_i(t) = [\tilde{y}_i^T(t) \int \tilde{y}_i^T(t)]^T$.

Then the closed-loop LFC model of the i^{th} area can be rewritten as

$$\begin{cases} \dot{x}_i(t)=A_ix_i(t)-B_iK_iC_ix_i(t_k-\tau(s_k))+F_i\omega(t) \\ y_i(t)=C_ix_i(t), \qquad\qquad\qquad t\in[t_k,t_{k+1}) \end{cases} \tag{7}$$

where

$$(A_i)_{5\times5}=\begin{bmatrix} \tilde{A}_i & 0 \\ \tilde{C}_i & 0 \end{bmatrix}, (B_i)_{5\times1}=\begin{bmatrix} \tilde{B}_i \\ 0 \end{bmatrix},$$

$$(C_i)_{2\times5}=\begin{bmatrix} \tilde{C}_i & 0 \\ 0 & 1 \end{bmatrix}, (F_i)_{5\times2}=\begin{bmatrix} \tilde{F}_i \\ 0 \end{bmatrix}, (K_i)_{1\times2}=\begin{bmatrix} 0 \\ K_{I,i} \end{bmatrix}^T.$$

Next, the ET communication scheme is revisited [31] here. The ET condition is defined as

$$\partial_1(j)=y_{ei}^T(s_{f_d+j})\varpi_iy_{ei}(s_{f_d+j})-\delta_iy_i^T(s_{f_d})\varpi_iy_i(s_{f_d})\leq0 \tag{8}$$

where $y_{ei}(s_{f_d+j})=y_i(s_{f_d+j})-y_i(s_{f_d})$ (j=1,2,...); $f_d(d=0,1,2,\ldots)$ are some integers; s_{f_d} represents the last event time; δ_i is a threshold parameter; and ϖ_i is a positive define weighting matrix.

Combining with $y_i(t)=C_ix_i(t)$, (8) can be rewritten as

$$\partial_2(j)=x_{ei}^T(s_{f_d+j})\Omega_ix_{ei}(s_{f_d+j})-\delta_ix_i^T(s_{f_d})\Omega_ix_i(s_{f_d})\leq0 \tag{9}$$

where $x_{ei}(s_{f_d+j})=x_i(s_{f_d+j})-x_i(s_{f_d})$ and $\Omega_i=C_i^T\varpi_iC_i$.

The next event-time instant $s_{f_{(d+1)}}$ is determined by

$$s_{f_{(d+1)}}=s_{f_d}+\min_{j\in\mathbb{N}}\{s_{f_d+j}-s_{f_d}|\partial_2(j)>0\} \tag{10}$$

Based on the ET scheme, the control law can be written as

$$u_i(t)=u_i(s_{f_d})=-K_iy_i(s_{f_d})=-K_iC_ix_i(s_{f_d}),\ t\in\Pi \tag{11}$$

where $\Pi=[t_{f_d},t_{f_{(d+1)}})$ with $t_{f_d}=s_{f_d}+\tau(s_{f_d})$. Similar to [31], the interval Π is divided into the following subsets Π_l,

$$\Pi=\cup\Pi_l,\ \ \Pi_l=[t_{f_d+l},t_{f_d+(l+1)}) \tag{12}$$

where $l=0,1,\ldots,f_{(d+1)}-f_d-1$, and

$$\tau(s_{f_d+l})=\begin{cases} \tau(s_{f_d}), l=0,1,\ldots,f_{(d+1)}-f_d-2 \\ \tau(s_{f_{(d+1)}}), l=f_{(d+1)}-f_d-1 \end{cases} \tag{13}$$

Define $\varsigma(t)=t-(t_{f_d+l}-\tau(s_{f_d+l}))$, $t\in\Pi_l$. The control law (11) can be rewritten as

$$u_i(t)=K_iC_i(x_{ei}(s_{f_d+l})-x_i(t-\varsigma(t))),\ t\in\Pi_l \tag{14}$$

Then, by replacing (6) with (14), the state-space model of delay-dependent ETLFC for a multi-area power system can be formulated as

$$\begin{cases} \dot{x}_i(t)=A_ix_i(t)+B_iK_iC_i(x_{ei}(s_{f_d+l})-x_i(t-\varsigma(t)))+F_i\omega_i(t) \\ y_i(t)=C_ix_i(t),\ t\in\Pi_l \end{cases} \tag{15}$$

The length of interval Π_l, $\bar{T}_{f_d+l}=t_{f_d+(l+1)}-t_{f_d+l}$, satisfies

$$0<\bar{h}_1\leq\bar{T}_{f_d+l}\leq\bar{h}_2<2h_2,\forall l\geq0. \tag{16}$$

where $\bar{h}_1=h_1-\min(\tau_M-\tau_m,\mu h_1)$ and $\bar{h}_2=h_2+\min(\tau_M-\tau_m,\mu h_2)$. Note that $|\dot{\tau}(t)|\leq\mu<1$ ensures that $|\tau(s_{f_d+(l+1)})-\tau(s_{f_d+l})|<\bar{T}_{f_d+l}$ and then, the sequence of t_{f_d+l} is strictly increasing. Moreover, for an isolated one-area LFC system, there will be no tie-line power. Therefore, the state-space model of the one-area LFC system will remove ΔP_{tie} from system (15).

III. CPS-BASED FUZZY EVENT-TRIGGERED LFC SCHEME

In this section, a CPS-based FET scheme is proposed for LFC of power systems with a limited communication bandwidth. The requirements of CPS1 and CPS2 of the NERC are first introduced. Then, a fuzzy control system is presented to adjust the control signal based on CPSs. Next, a stability condition of the ET LFC system with the participation of the fuzzy control system is obtained, and the method of dynamically adjusting the threshold parameters of the ET scheme based on the function expression is given. Finally, the design procedure of the proposed scheme is summarized.

A. CPSs

For equitable operation of the interconnected system, control areas have to comply with the NERC's CPS1 and CPS2, which were adopted in February 1997. Each control area is required to monitor its control performance and report its compliance with CPS1 and CPS2 to the NERC at the end of each month ([35]). CPS1 and CPS2 and the relationship between them are described below.

CPS1 assesses the impact of the ACE on frequency over a 12-month window or horizon and is expressed as

$$CPS1_i=(2-CF_{sum-i})\times100\% \tag{17}$$

where $CF_{sum-i}=AVG_{12-month}[(CF_i)_1]$ is the compliance factor of area i, and is defined as the average of all $(CF_i)_1$ during a 12-month period, and $(CF_i)_1$ is defined as follows:

$$(CF_i)_1=\left[\left(\frac{ACE_i}{\beta_i}\right)_1\left(\frac{\Delta f_i}{\varepsilon_1^2}\right)_1\right] \tag{18}$$

where ε_1 represents the targeted frequency bound for CPS1 and $(\cdot)_1$ is the clock-1-min average. To comply with NERC, CPS1 should not be less than 100%.

CPS2 requires the 10-min averages of a control area's ACE to be less than a constant (L_{10-i}) given in the equation below.

$$(ACE_i)_{10min}\leq L_{10-i}=1.65\varepsilon_{10}\sqrt{\beta_i\beta_s} \tag{19}$$

where$(ACE_i)_{10min}$ is the 10-min average of the area's ACE, β_s is the summation of the frequency bias of all control areas in the considered interconnection, and ε_{10} is the targeted frequency bound for CPS2. To comply with this standard, each control area needs to have its compliance no less than 90%. A compliance percentage is calculated by the following equation

$$CPS2_i=100\left(1-\frac{Num((ACE_i)_{10min}>L_{10-i})}{Num(all|(ACE_i)_{10min})}\right)\% \tag{20}$$

where $Num((ACE_i)_{10min}>L_{10-i})$ denotes the number of $(ACE_i)_{10min}$ that satisfies $(ACE_i)_{10min}>L_{10-i}$ in one month, and $Num(all|(ACE_i)_{10min})$ represents the number of all $(ACE_i)_{10min}$ in one month.

As stated in [16], under certain conditions that generally hold, the satisfaction of CPS1 implies that CPS2 is also fulfilled. As such, CPS2 is a redundant criterion. Once CPS1 is satisfied, it becomes unnecessary to check CPS2. The conditions are shown as follows:

(1) the average ACE random variables of each control area are independent; and
(2) the averages of these random variables are zero.

These conditions are assumed to hold in this paper and the fuzzy logic rules are designed to comply with CPS1 only. This reduces the complexity of fuzzy rule design.

B. CPS-based fuzzy control system design

A fuzzy control system is employed to manipulate the ACE_i of each area to achieve two objectives: (i) minimize wear and tear on generating unit equipment and (ii) comply with the NERC's CPS1 and CPS2. The manipulated ACE is defined as

$$ACE_{i,m} = \alpha_i ACE_i \tag{21}$$

where α_i is calculated by fuzzy logic rules and called fuzzy gain with $\alpha_i \in (0,1)$. Then, one can rewrite the control structure for each area in the form:

$$\begin{aligned}\tilde{u}_i(t) = \Delta P_{ci}(t) &= -K_{I,i}\int ACE_{i,m}(t)dt \\ &= (-\alpha_i K_{I,i})\int ACE_i(t)dt\end{aligned} \tag{22}$$

It can be seen that the changes in ACE_i through fuzzy logic rules can be transformed into the changes in the integral gains of $K_{I,i}$. The proposed fuzzy logic will lower the control gains when the control area has high compliance. On the other hand, the control gains will be increased when the compliance factor of CPS1 is low. The detailed descriptions of the fuzzy control system are shown as follows.

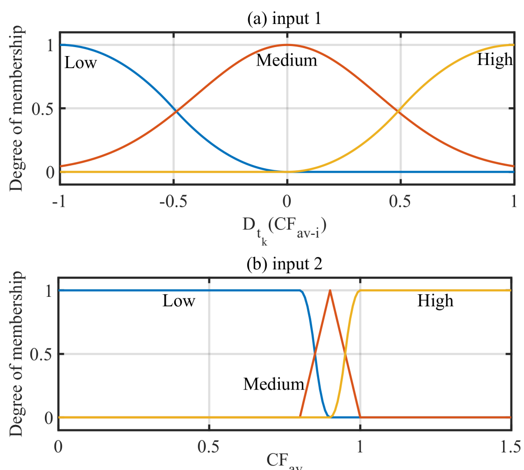

Fig. 2. Input membership functions in fuzzy control.

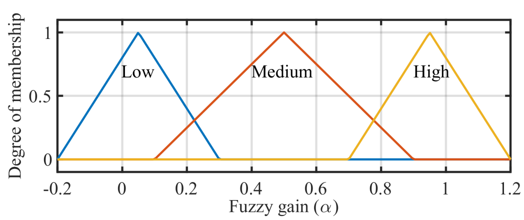

Fig. 3. Output membership functions in fuzzy control.

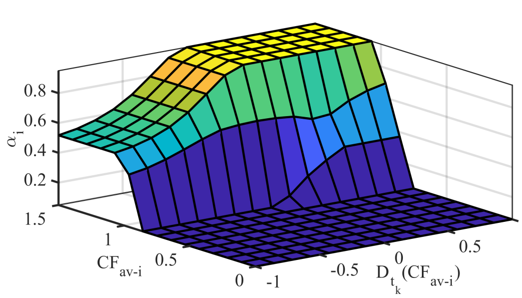

Fig. 4. Relationship of fuzzy system inputs and output.

The inputs for the fuzzy control system are the accumulative average compliance factor CF_{av-i} and its change rate $D_{t_k}(CF_{av-i})$ defined in the following equations (23) and (24), respectively.

$$CF_{av-i} = AVG_{X\rightarrow Y}[(CF_i)_1] \tag{23}$$

where points X and Y represent the start and end of the 12-sliding-month period, respectively. At sliding point Y, CF_{av-i} is calculated every minute, and each control area is required to record its level of compliance with CPSs.

$$D_{t_k}(CF_{av-i}) = ((CF_{av-i})_{t_k} - (CF_{av-i})_{t_{k-1}})/(CF_{av-i})_{t_{k-1}} \tag{24}$$

where t_j with $j = 0, 1, 2, \cdots$ denotes the time when (CF_{av-i}) is calculated every minute and t_k represents the current time. The output of the fuzzy control system is the fuzzy gain α_i. The inputs and output membership functions are shown below. Fig. 2 describes (CF_{av-i}) and its change rate $D_{t_k}(CF_{av-i})$, and Fig. 3 depicts fuzzy gain α_i.

The fuzzy rule concepts are summarized in Table I. Once the inputs are determined, the output, i.e., the fuzzy gain, can be obtained. Fig. 4 describes the relationship of the inputs and output of the fuzzy control system through a $3-D$ mesh surface.

TABLE I
FUZZY LOGIC RULES FOR TUNING FUZZY GAINS

$D_{t_k}(CF_{av-i})$	Operator	CF_{av-i}	α_i
Low or Medium or High	and	Low	Low
Low or Medium	and	Medium	Low
High	and	Medium	Medium
Low	and	High	Medium
Medium or High	and	High	High

It is worth noting that in the simulation test, the actual data during a 12-month period will be difficult to obtain. For convenience, assume that 1000 sets of $(CF_i)_1$ have been collected before starting the simulation test, and their average is set to CF_{s-i}. The 1-minute average of the data of $(CF_i)_1$ obtained from the simulation test and the 1000 sets of $(CF_i)_1$ are then calculated and used as the above CF_{av-i} for the input to the fuzzy control system.

C. Adjustable ET condition based on the stability condition

Based on equation (22) and the LFC system model (15), one can derive the following theorem to guarantee the fuzzy event-triggered LFC system stability.

Theorem 1: Consider system (15) with zero disturbance and r the dimension of matrix A_i in system (15). For given $T_k \in [h_1, h_2]$, $\tau_i \in [\tau_m, \tau_M]$ with $|\dot{\tau}_i(t)| \le \mu < 1$, δ_i, α_i and K_i, system (15) is asymptotically stable if there are positive definite symmetric matrices $P\in \mathbb{R}^{3r\times 3r}$, $M\in \mathbb{R}^{r\times r}$, $N\in \mathbb{R}^{r\times r}$, $H\in \mathbb{R}^{r\times r}$, $R_1\in \mathbb{R}^{2r\times 2r}$, $R_2\in \mathbb{R}^{2r\times 2r}$ and $\Omega_i\in \mathbb{R}^{r\times r}$, and any matrices $Q_1\in \mathbb{R}^{4r\times 4r}$, $Q_2\in \mathbb{R}^{4r\times 4r}$, $X\in \mathbb{R}^{2r\times 2r}$, $Z\in \mathbb{R}^{4r\times 4r}$, $U_1\in \mathbb{R}^{9r\times 2r}$ and $U_2\in \mathbb{R}^{9r\times 2r}$, such that, for $j = 1, 2$, satisfy the following inequalities hold:

$$\Xi_1 = \begin{bmatrix}\Theta_1 + \bar{h}_j\Theta_2 & \bar{h}_j U_2 \\ * & -\bar{h}_j R_2\end{bmatrix} < 0 \tag{25}$$

$$\Xi_2 = \begin{bmatrix}\Theta_1 + \bar{h}_j\Theta_3 & \bar{h}_j U_1 \\ * & -\bar{h}_j R_1\end{bmatrix} < 0 \tag{26}$$

where

$$
\begin{aligned}
\Theta_1 =& e_1^T M e_1 - e_2^T M e_2 + E_0^T N E_0 - e_3^T N e_3 + \tau_M E_0^T H E_0 \\
& - \frac{1}{\tau_M}\Pi_3^T \begin{bmatrix} H & 0 \\ 0 & 3H \end{bmatrix} \Pi_3 + Sym\{\Pi_1^T P \Pi_{21} + \Pi_{71}^T Q_1 \Pi_{72} \\
& + \Pi_{71}^T Q_2 \Pi_8 + \Pi_2^T X(\Pi_4 - \Pi_6) + (\Pi_4 - \Pi_5)^T X \Pi_2 \\
& - U_1(\Pi_4 - \Pi_5) + U_2(\Pi_4 - \Pi_6)\} \\
& + \delta_i (e_5 - e_9)^T \Omega_i (e_5 - e_9) - e_9^T \Omega_i e_9 \\
\Theta_2 =& Sym\left\{ \begin{bmatrix} \Pi_2 \\ 0 \end{bmatrix}^T Q_1 \Pi_{72} + \begin{bmatrix} \Pi_4 - \Pi_5 \\ 0 \end{bmatrix}^T Q_1 \begin{bmatrix} \Pi_2 \\ \Pi_2 \end{bmatrix} \right\} \\
& + Sym\left\{ \begin{bmatrix} \Pi_2 \\ 0 \end{bmatrix}^T Q_2 \Pi_8 \right\} + \Pi_8^T Z \Pi_8 + \Pi_2^T R_1 \Pi_2 \\
\Theta_3 =& Sym\left\{ \begin{bmatrix} 0 \\ \Pi_2 \end{bmatrix}^T Q_1 \Pi_{72} + \begin{bmatrix} 0 \\ \Pi_4 - \Pi_6 \end{bmatrix}^T Q_1 \begin{bmatrix} \Pi_2 \\ \Pi_2 \end{bmatrix} \right\} \\
& + Sym\left\{ \begin{bmatrix} 0 \\ \Pi_2 \end{bmatrix}^T Q_2 \Pi_8 \right\} - \Pi_8^T Z \Pi_8 + \Pi_2^T R_2 \Pi_2 \\
E_0 =& A e_1 + \alpha_i B_i K_i C_i (e_9 - e_5),\ \Pi_1 = [e_1^T\ e_2^T\ \tau_M e_8^T]^T \\
\Pi_2 =& [E_0^T\ e_3^T]^T,\ \Pi_{21} = [\Pi_2^T\ (e_1 - e_2)^T]^T \\
\Pi_3 =& [(e_1 - e_2)^T\ (e_1 + e_2 - 2e_8)^T]^T \\
\Pi_4 =& [e_1^T\ e_2^T]^T,\ \Pi_5 = [e_4^T\ e_5^T]^T,\ \Pi_6 = [e_6^T\ e_7^T]^T \\
\Pi_{71} =& [(\Pi_5 - \Pi_4)^T\ (\Pi_4 - \Pi_6)^T]^T \\
\Pi_{72} =& [(\Pi_4 - \Pi_5)^T\ (\Pi_4 - \Pi_6)^T]^T,\ \Pi_8 = [\Pi_5^T\ \Pi_6^T]^T \\
e_i =& [0_{r\times(i-1)r}\ \ I_r\ \ 0_{r\times(9-i)r}],\ i = 1, 2, \cdots 9.
\end{aligned}
$$

with $\bar{h}_1$ and $\bar{h}_2$ defined in (16) and denoting $Sym\{\mathbb{A}\} = \mathbb{A} + \mathbb{A}^T$. The proof can be found in Appendix.

Under the given $K_{I,i}$ and α_i, the following algorithm is used to obtain the maximum threshold parameters that the system can withstand.

Algorithm 1: Find the maximum threshold parameter $\delta_{i,m}$.

Step 1 Preset system parameters: $\tau_m, \tau_M, \mu, h_1, h_2$, and α_i; system matrices A_i, B_i, C_i and K_i.

Step 2 Initialize the search interval $[\delta_{min}, \delta_{max}]$ with $\delta_{min} = 0$ and large enough number δ_{max} and select the accuracy coefficient $\delta_{ac} = 0.0001$.

Step 3 Check the feasibility of LMIs (25) and (26) under $\delta_{test} = (\delta_{min} + \delta_{max})/2$. If (25) and (26) are feasible, set $\delta_{min} = \delta_{test}$; else, set $\delta_{max} = \delta_{test}$.

Step 4 If $|\delta_{min} - \delta_{max}| \le \delta_{ac}$, obtain $\delta_{i,m} = \delta_{min}$, output $\delta_{i,m}$. If $\delta_{i,m} = 0$, no feasible solution.

Note that the fuzzy gains will be updated every minute according to the above CPS-based fuzzy logic rules. Based on Algorithm 1, we can reset the threshold parameter of the ET condition in real time by using the calculated $\delta_{i,m}$. However, when the algorithm is used in higher-dimensional systems, Algorithm 1 may spend a significant time calculating $\delta_{i,m}$ and may not be able to update the threshold parameter within one minute. To solve this problem, the processing method calculates the maximal threshold parameters under a given controller gain and different fuzzy gains in advance based on Algorithm 1 and then determines the function expression of the threshold parameter δ, the controller gain $K_{I,i}$ and the fuzzy gain α_i by means of a curve fitting method in MATLAB. Finally, the threshold parameters can be calculated in real time through their function expression under a given controller gain $K_{I,i}$ and fuzzy gain α.

Remark 1: CPS1 is a statistical average standard. In the CPS-based event-triggered LFC scheme in [34], each compliance factor $(CF_i)_1$ is requested to satisfy CPS1, ignoring the statistical average characteristics. In contrast, the proposed CPSFET scheme is based on the average of each compliance factor $(CF_i)_1$ to adjust the fuzzy gain and then change the threshold parameter of the event-triggered communication scheme. Therefore, considering the statistical characteristics, the proposed CPSFET scheme has the ability to improve the selection of threshold parameters and further reduce the triggering frequency of signals.

Remark 2: Compared with the general fuzzy-based LFC scheme in [26, 27], the proposed CPSFET LFC scheme considers the update period of control signal, which ensures the stable operation of the proposed LFC scheme under a large sampling period. In addition, the proposed control scheme introduces the event-triggered communication scheme, which greatly reduces the measurement and control signal transmission in the network and reduces the usage of communication bandwidth.

Remark 3: The fuzzy gain output by the fuzzy control system is used to change the control input of the governor and the threshold parameter of the event-triggered communication scheme. Then, compared with the general LFC scheme without fuzzy control in [31, 34], the proposed LFC scheme based on fuzzy control has two advantages: reducing the control input of the governor to reduce wear and tear on the generating unit equipment and improving the selection of the threshold parameter as well as reducing the signal triggering frequency to further reduce the usage of communication bandwidth.

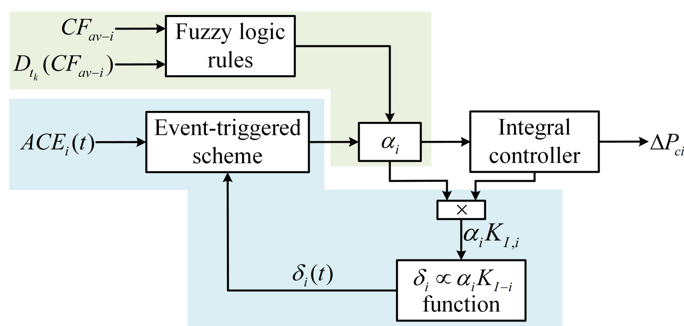

Fig. 5. Schematic of the CPS-based fuzzy ET LFC scheme.

D. Summary of the CPS-based FET LFC scheme

Based on the above descriptions, the CPS-based FET LFC scheme can be divided into two aspects: the CPS-based fuzzy control system and the function expression-based adjustable event-triggered communication scheme. A schematic of the proposed scheme is shown in Fig. 5. Algorithm 2 is introduced to summarize the design procedure of the proposed scheme.

Algorithm 2

Step 1 Divide power systems into N control areas. Initialize i^{th} control area system matrices: A_i, B_i, C_i, and K_i; and the system parameters: $\tau_m, \tau_M, \mu, h_1, h_2$, and CF_s.

Step 2 Construct ET LFC model and derive its stability condition.

Step 3 Construct fuzzy control system. Based on Algorithm 1 and the curve fitting method, obtain the function expression of $\alpha_i K_{Ii}$ and δ_i. Based on the CF_s, calculate the initial fuzzy gain $\alpha_{i,0}$ by fuzzy control system and the initial threshold parameter $\delta_{i,0}$ by the function expression.

Step 4 Measure Δf_i and ΔP_{tie-i}, and calculate CF_{av-i} and $D_{t_k}(CF_{av-i})$. Set CF_{av-i} and $D_{t_k}(CF_{av-i})$ as the inputs of the fuzzy control system and output the fuzzy gain α_i.

Step 5 According to the obtained function curve and α_i, derive δ_i and update the ET condition.

Step 6 Based on ET condition, evaluate whether trigger ACE signal. Modify the triggered ACE signal by fuzzy gain α_i, and obtain the control signal ΔP_{ci} by integral controller. Input the control signal into the governor. Repeat Steps 4-6.

Remark 4: In the design of the proposed LFC scheme, the controller parameters are given in advance, as shown in Step 1 of Algorithm 2. In the fuzzy control system, the parameters that need to be calculated only include the fuzzy control output, i.e., the fuzzy gain. With the real-time measurements input to the fuzzy control system, the output fuzzy gain is calculated by the fuzzy rules shown in Table I. Then, the calculated fuzzy gain is used to change the area control error of the LFC system and thus adjust the control signal, as shown in equations (21) and (22).

IV. Case studies

In this section, case studies are undertaken based on a one-area LFC system and an IEEE 39-bus benchmark test system to show the effectiveness and advantages of the proposed CPS-based FET LFC scheme.

A. One-area LFC system

1) Design of the CPSFET LFC scheme: The parameters of the one-area LFC system are shown in Table II. Then, based on the representation of system (7), the initial system matrices in Algorithm can be determined by:

$$A = \begin{bmatrix} -0.1 & 0.1 & 0 & 0 \\ 0 & -10 & 10 & 0 \\ -66.67 & 0 & -3.33 & 0 \\ 21.0 & 0 & 0 & 0 \end{bmatrix},$$

$$B = \begin{bmatrix} 0 & 0 & 3.33 & 0 \end{bmatrix}^T, C = \begin{bmatrix} 21 & 0 & 0 & 0 \\ 0 & 0 & 0 & 1 \end{bmatrix}.$$

Additionally, the integral gain in the studied system is assumed to be $K_I = 0.2$. That is, the control matrix is $K = [0, 0.2]$.

TABLE II
Parameters of the one-area LFC system

T_{ch}(s)	T_g(s)	R(Hz/pu)	D(pu/Hz)	M(pu·s)	β(pu/Hz)
0.30	0.10	0.05	1.0	10	21.0

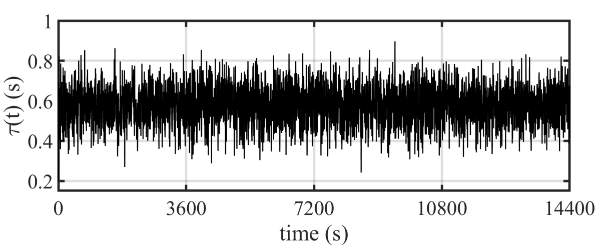

Fig. 6. Details of the uncertain time delay $\tau(t)$.

The initial parameters are set as $\tau_m = 0.15, \tau_M = 1, \mu = 0.5$, $h_1 = 2$, $h_2 = 4$, and $CF_s = 0.92$. That is, the sampling period of the system is $T_k \in [2, 4]$ s; the time delay is $\tau(t) \in [0.15, 1]$ s with $|\dot{\tau}(t)| \leq 0.5$ [42]; the initial average of $(CF)_1$ is set as $CF_s = 0.92$. In the simulation tests, the time delay is not expressed by a specific expression. Instead, a random signal generator is used to generate the random time delays at every sampling time, and the upper bound and lower bound of the signal generator are set as 0.15 and 1, respectively, as the boundaries of the time delay. Then, using a slope limiter limits the rate of change of the random signal, which guarantees that the derivative condition of $|\dot{\tau}(t)| \leq 0.5$ is met. The details of the time delays are plotted in Fig. 6.

Following the steps of Algorithm 2, the function expression of the fuzzy gains and the threshold parameters is obtained, $L : \delta = 1.316exp(-((\alpha K_I + 0.08083)/0.1422)^2) + 0.139exp(-((\alpha K_I - 0.1139)/0.09216)^2)$. The fitting curve L is depicted in Fig. 7. Then, the initial fuzzy gain and threshold parameter are obtained as $\alpha_0 = 0.174$ and $\delta_0 = 0.745$, respectively.

Under the above initial conditions, the one-area LFC is simulated. Additionally, for convenience, the sampling period is set to a fixed and maximum value, that is, $T_k = 4$s.

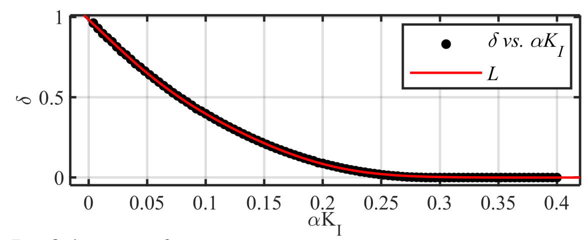

Fig. 7. fitting curve for one-area power system.

2) Simulation tests: To demonstrate the advantages of the proposed CPS-based FET (CPSFET) LFC scheme, the following general non-fuzzy-based LFC schemes and CPS-based fuzzy LFC scheme are compared in the following simulation tests.

a) The conventional time-triggered (TT) LFC scheme;
b) The ET LFC scheme in [30];
c) The adaptive ET (AET) LFC scheme in [31];
d) The CPS oriented ET (CPSET) LFC scheme in [34];
e) The CPS-based fuzzy LFC (FLFC) scheme in [26, 27].

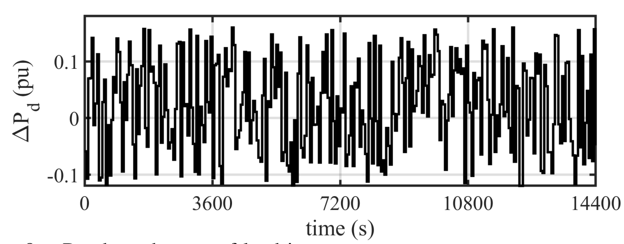

Fig. 8. Random changes of load in one-area power system.

TABLE III
Amounts of signal transmission in different control schemes

Schemes	CPSFET	CPSET	AET	ET	TT
Amounts	611	887	1240	1246	3600

Under the above six schemes, the studied system is tested with random changes in load within four hours. The changes in load ΔP_d are shown in Fig. 8. The responses of the frequency deviation and the control input of the studied system under the different control schemes are displayed in Figs. 9 (a) and (b), respectively. The changes in threshold parameters in the CPSET, AET and CPSFET LFC schemes are plotted and compared in Fig. 10. To show the ability to reduce the communication network bandwidth, the triggering moments of ACE signals in the CPSET, AET and CPSFET LFC schemes are shown in Fig. 11. In detail, the amounts of ACE signal transmission in different control schemes are listed in Table III. The fuzzy gains α of CPSFET and FLFC automatically change according to the control area's percentage of compliance with CPS1 and are plotted in Fig. 12. Additionally, $(CF)_1$ of every minute and the aggregative 1-minute average CF_{av} of all $(CF)_1$ are shown in Figs.13 (a) and (b), respectively. The 10-minute averages of the ACE are calculated and compared with the constants L_{10} in Fig. 14.

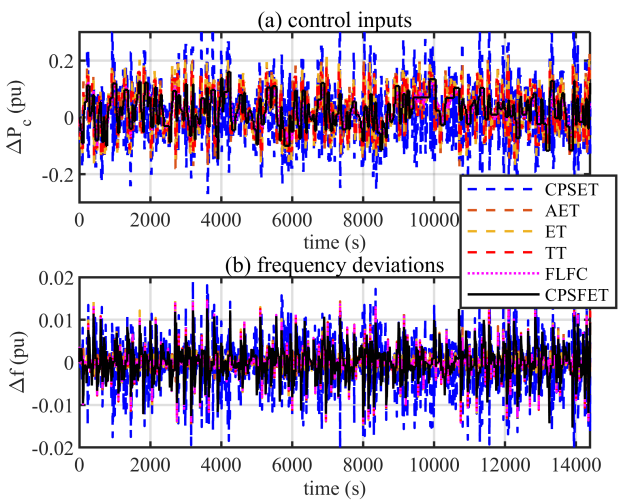

Fig. 9. Control inputs and frequency deviations of one-area power system.

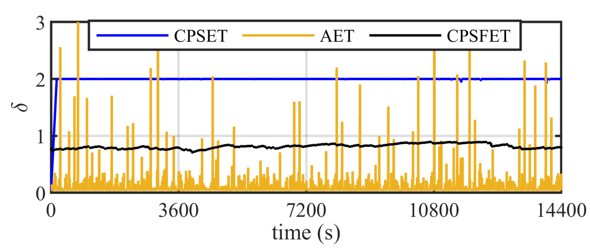

Fig. 10. Threshold parameters of one-area power system.

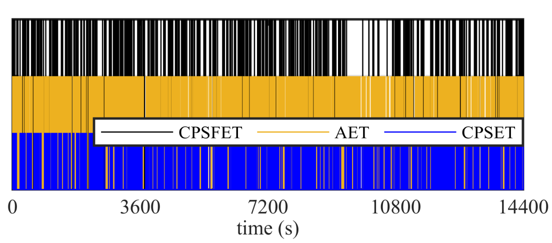

Fig. 11. Triggering time in CPSET, AET, and CPSFET LFC schemes.

It can be seen from Fig. 9 (a) that the CPS-based fuzzy LFC schemes (including the general FLFC and the proposed CPSFET scheme) can generate smaller control inputs to the governor than other non-fuzzy-based LFC schemes. Additionally, the proposed CPSFET scheme will not change the frequency response dramatically and does not cause greater frequency deviation. To comply with the NERC, CPS1 should not be less than 100%. Based on equation (17), the aggregative 1-minute average CF_{av} of $(CF)_1$ should not be more than 1. As shown in Fig. 13(b), these results all comply with the CPS1 requirement. According to CPS2, the 10-minute averages of the ACE must be equal to or less than L_{10} at least 90% of times. Based on the results in Fig. 14, all 10-min averages are less than its standard constant L_{10}. These results are also in compliance with CPS2. From Fig. 13, differences between the CPS-based fuzzy LFC and non-fuzzy-based LFC schemes can be clearly found. Under the CPS-based fuzzy LFC schemes, $(CF)_1$ is not always less than 1, and the aggregative 1-minute average CF_{av} also fluctuates around a fixed value that just satisfies CPS1. This is the advantage of considering the statistical characteristics in CPS-based fuzzy LFC schemes since the CPS1 is actually a statistical average standard. In the statistical average, it is not required that every element for which the average is calculated satisfies the CPS1 requirement; only their average needs to satisfy the requirement. Therefore, these non-fuzzy control schemes, TT, ET, AET, and CPSET, where the statistical characteristics are not considered lead to a continuous decline of CF_{av} and excessively meet the CPS1 requirement.

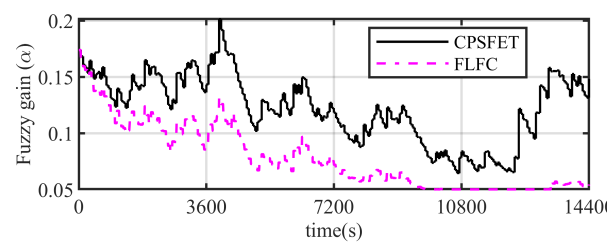

Fig. 12. Changes of fuzzy gain in fuzzy logic rules of one-area power system.

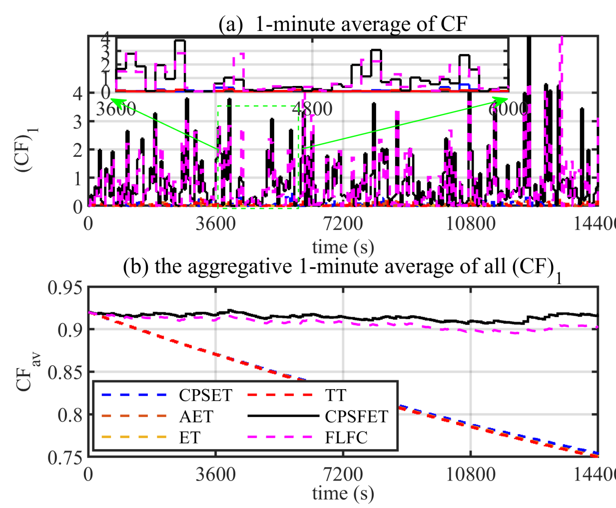

Fig. 13. CF_1 and CF_{av} of one-area power system.

On the other hand, moving on to Fig. 10, it can be observed that the proposed scheme can generate smooth threshold parameters to update the event-triggered condition. Although the threshold parameters in the proposed scheme are mostly less than those in the CPSET and AET LFC schemes, the proposed scheme can further reduce unnecessary signal transmission compared to other schemes, as shown in Fig. 11 and Table III. Specifically, the following equation is given to calculate the improvement ratio:

$$\nu_r = \frac{n_2 - n_1}{n_2} \times 100\% \tag{27}$$

where n_1 represents the transmission amount of the ACE signal in the proposed CPSFET LFC scheme, and n_2 denotes the transmission amount of the ACE signal in the existing LFC schemes. Compared with the traditional TT LFC scheme, the amount of signal transmission is reduced by 83.03%, while it is reduced by 31.12% compared with the optimal CPSET LFC scheme among the existing control schemes.

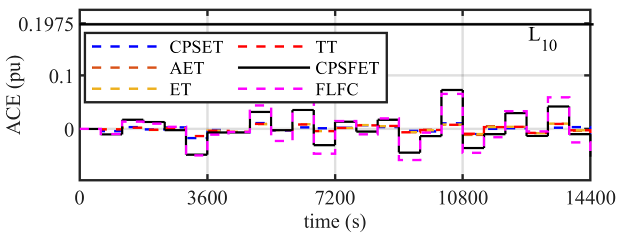

Fig. 14. 10-minutes average of ACE of one-area power system.

The test results from the one-area LFC system indicate that the proposed CPSFET LFC scheme can meet the requirements of CPS1 and CPS2 and not only inherits the advantage of the CPS-based FLFC scheme in [26, 27] in reducing the wear and tear on generating unit equipment but also further lowers the usage of communication bandwidth in comparison with the non-fuzzy control schemes [31, 34].

3) Simulation tests under different initial CF_s values: When the initial CF_s is different, the control process of the CPSFET LFC system also varies. Therefore, in this part, we will show the effectiveness and difference of the proposed scheme under different initial CF_s values. In the following tests, assume that CF_s is set as 1.1, 0.92 and 0.8. Under the action of the proposed scheme, the one-area LFC system is simulated with the random changes in load shown in Fig. 8 within five hours.

The control inputs and the frequency deviations of the studied system are plotted in Figs. 15 (a) and (b), respectively. The fuzzy gains α and the changes in threshold parameters δ are depicted in Figs. 16 (a) and (b), respectively. Additionally, $(CF)_1$ and the aggregative 1-minute average CF_{av} are shown in Figs.17 (a) and (b), respectively.

It can be seen from Figs. 16 (a) and (b) that when the initial CF_s is higher than 1 and the CPS1 requirement is not met, the fuzzy gains α reach the maximum and the threshold parameters δ are at the minimum to maximize the control inputs and increase the update frequency of the control signal. The fuzzy gains α are reduced and the threshold parameters δ are increased until the control performance of the studied system complies with CPS1. In contrast, when the initial CF_s is 0.8 and the CPS1 requirement is overly satisfied, the fuzzy control gains α are at the minimum and the threshold parameters reach the maximum to minimize the control inputs and reduce the update frequency of the control signal to the maximum extent. When $CF_s = 0.92$ and the

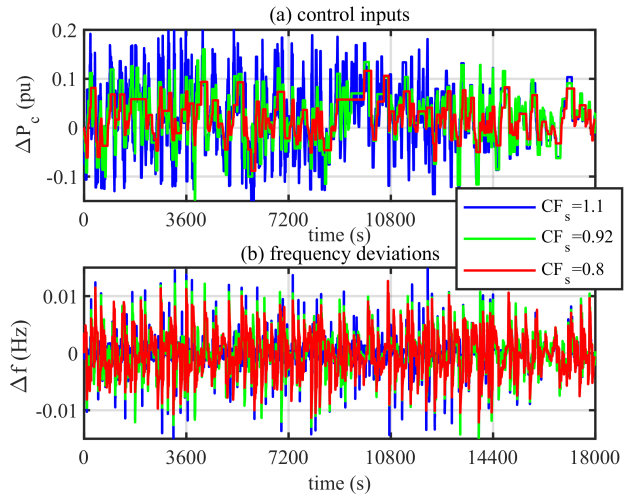

Fig. 15. Control inputs and frequency deviations of one-area power system.

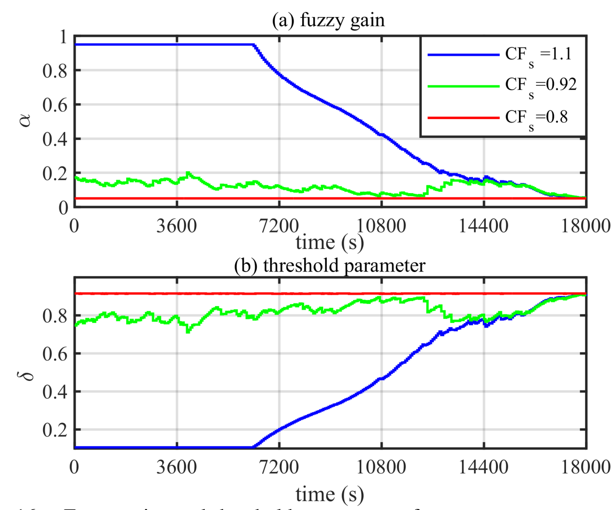

Fig. 16. Fuzzy gains and threshold parameters of one-area power system.

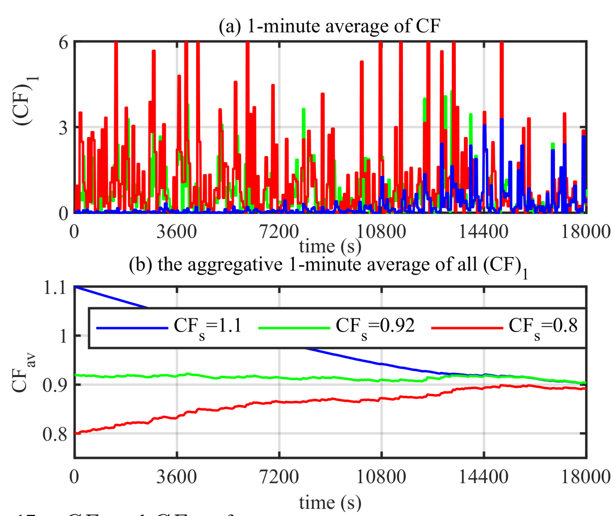

Fig. 17. CF_1 and CF_{av} of one-area power system.

CPS1 requirement is just met, the fuzzy gains and threshold parameters will gently fluctuate up and down to maintain the aggregative 1-minute average CF_{av} of $(CF)_1$ fluctuating around 0.92. Fig. 15 (a) reflects a lower initial value, resulting in smaller control inputs and lower update frequency of the control signal. As shown in Fig. 15 (b), a higher initial value will make the system frequency change more dramatic and the peak value of the frequency deviation larger. Additionally, it can be observed from Fig. 17 (a) that when the initial value is high, most of $(CF)_1$ is less than 1, reducing the aggregative 1-minute average CF_{av} and reaching the specified requirement of CPS1. When the initial value is low, $(CF)1$ will mostly be higher than 1 to increase the aggregative 1-minute average CF_{av} and just meet the CPS1 requirement. These results demonstrate the effectiveness of the proposed scheme under different CF_s values.

B. IEEE 39-bus benchmark test system

To investigate the feasibility of the proposed approach in a complex power system, case studies are undertaken based on an IEEE 39-bus benchmark test system. The system comprises 10 generators, 19 loads, 34 transmission lines, and 12 transformers. The generators are equipped with excitation and power system stabilizer units.

1) Design of the CPS-based FET LFC scheme: The IEEE 39-bus benchmark system is divided into three control areas. Assume that every generator in each control area is responsible for the secondary frequency regulation task. The parameters for the generators, loads, lines and transformers are given in [36]. The single-line diagram of the IEEE 39-bus benchmark test system can be found in [34], and the parameters used in the LFC scheme design are given in Table IV. To simplify the calculation, in every control area, all generators are equivalent to one generator. Then, based on the representation of system (7), the initial system matrices can be determined by:

$$A_1 = \begin{bmatrix} 0 & -0.0431 & 0.0431 & 0 & 0 \\ 10.96 & 0 & 0 & 0 & 0 \\ 0 & 0 & -10 & 10 & 0 \\ -200 & 0 & 0 & -3.33 & 0 \\ 60 & 1 & 0 & 0 & 0 \end{bmatrix},$$

$$A_2 = \begin{bmatrix} 0 & -0.0432 & 0.0432 & 0 & 0 \\ 4.4768 & 0 & 0 & 0 & 0 \\ 0 & 0 & -5.8824 & 5.8824 & 0 \\ -228.5714 & 0 & 0 & -2.8571 & 0 \\ 80 & 1 & 0 & 0 & 0 \end{bmatrix},$$

$$A_3 = \begin{bmatrix} 0 & -0.0496 & 0.0496 & 0 & 0 \\ 10.1982 & 0 & 0 & 0 & 0 \\ 0 & 0 & -5 & 5 & 0 \\ -150 & 0 & 0 & -2.5 & 0 \\ 60 & 1 & 0 & 0 & 0 \end{bmatrix},$$

$$B_1 = \begin{bmatrix} 0 & 0 & 0 & 3.33 & 0 \end{bmatrix}^T, C_1 = \begin{bmatrix} 60 & 1 & 0 & 0 & 0 \\ 0 & 0 & 0 & 0 & 1 \end{bmatrix},$$

$$B_2 = \begin{bmatrix} 0 & 0 & 0 & 2.8571 & 0 \end{bmatrix}^T, C_2 = \begin{bmatrix} 80 & 1 & 0 & 0 & 0 \\ 0 & 0 & 0 & 0 & 1 \end{bmatrix},$$

$$B_3 = \begin{bmatrix} 0 & 0 & 0 & 2.5 & 0 \end{bmatrix}^T, C_3 = \begin{bmatrix} 60 & 1 & 0 & 0 & 0 \\ 0 & 0 & 0 & 0 & 1 \end{bmatrix}.$$

Additionally, the integral controller gains in each control area are assumed to be equal, and $K_{I,1} = K_{I,2} = K_{I,3} = 0.2$. That is the controller matrices are $K_1 = K_2 = K_3 = [0, 0.2]$.

The initial parameters in every control area are set as $\tau_m = 0.15, \tau_M = 1, \mu = 0.5$, $h_1 = 2$, $h_2 = 4$, and $CF_s = 0.92$. That is, the sampling period of the system is $T_k \in [2, 4]$ s; the time delay is $\tau(t) \in [0.15, 1]$ s with $|\dot{\tau}(t)| \leq 0.5$; the initial average of $(CF_i)_1$ is set as $CF_{s-i} = 0.92$ with $i = 1, 2, 3$. The details of time delay $\tau(t)$ are plotted in Fig. 6.

TABLE IV
LFC SYSTEM PARAMETERS IN IEEE 39-BUS BENCHMARK TEST SYSTEM

	Control area 1			Control area 2				Control area 3		
Generator	G1	G2	G3	G4	G5	G6	G7	G8	G9	G10
$T_g(s)$	0.1	0.1	0.1	0.17	0.17	0.17	0.17	0.2	0.2	0.2
$T_{ch}(s)$	0.3	0.3	0.3	0.35	0.35	0.35	0.35	0.4	0.4	0.4
α	0.33	0.33	0.33	0.25	0.25	0.25	0.25	0.33	0.33	0.33
R(Hz/pu)	0.05	0.05	0.05	0.05	0.05	0.05	0.05	0.05	0.05	0.05
M(pu·s)	10	6.06	7.16	5.72	5.20	6.96	5.28	4.86	6.90	8.40
D(pu/Hz)	0	0	0	0	0	0	0	0	0	0
β(Hz/pu)	20	20	20	20	20	20	20	20	20	20
$T_{ij}(s)$(pu/rad)	$T_{12} = 0.4166, T_{13} = 1.3272, T_{23} = 0.2959$									

Following Algorithm 2, the threshold parameters δ_i with $i = 1, 2, 3$ in every control area corresponding to $\alpha_i K_I$ can be calculated based on Algorithm 1, and then, the Guassian-type curve fitting method in MATLAB is used to obtain their function expression L_i, $L_1 : \delta_1 = 1.063exp(-((\alpha_1 K_{I,1} + 0.08906)/0.1784)^2)$, $L_2 : \delta_2 = 1.209exp(-((\alpha_2 K_{I,2} + 0.1003)/0.1592)^2)$ and $L_3 : \delta_3 = 1.302exp(-((\alpha_3 K_{I,3} + 0.1085)/0.1717)^2)$. The fitting curves L_i with $i = 1, 2, 3$ obtained are plotted in Fig. 18. Then, the initial fuzzy gain and threshold parameter in every control area are obtained as $\alpha_{1,0} = \alpha_{2,0} = \alpha_{3,0} = 0.174$ and $\delta_{1,0} = 0.656, \delta_{2,0} = 0.588$ and $\delta_{3,0} = 0.649$, respectively.

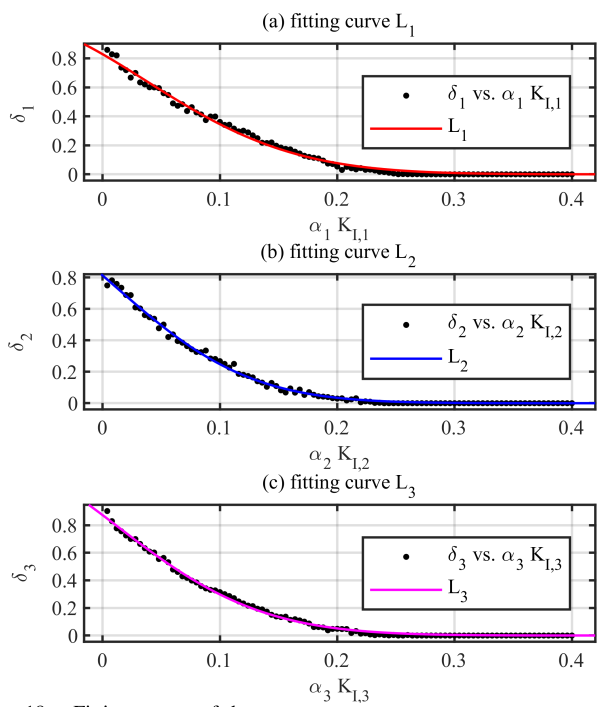

Fig. 18. Fitting curves of three areas.

Under the above initial conditions, the IEEE 39-bus benchmark test system is simulated. Similar to the above simulation tests in the one-area power system, the sampling period is set to a maximum of 4 s for convenience in the following tests. Additionally, the generation rate constraints for every generator are considered to be ± 0.1 pu/min.

2) Simulation tests and evaluations: To demonstrate the advantages of the proposed CPS-based FET (CPSFET) LFC scheme in reducing wear and tear on the generating unit equipment and saving communication network bandwidth, the following non-fuzzy-based LFC schemes are compared in the following simulation tests:

a) The conventional TT LFC scheme;
b) The ET LFC scheme in [30];
c) The AET LFC scheme in [31];
d) The CPSET LFC scheme in [34].

Following the steps in Algorithm 2, the CPSET, AET, ET, TT and proposed CPSFET LFC schemes are applied to the studied system. Under $T_k = 4$ s and $\tau = [0.15, 1]$ s with $|\dot{\tau}(t)| \leq 0.5$, the system is tested with random changes in load within four hours. The changes in load are shown in Fig. 19.

The responses of the control inputs and the frequency deviations of area 3 under different control schemes are plotted in Figs. 20 (a) and (b), respectively. The changes in threshold parameters and the triggering time of ACE signals in the CPSET, AET and CPSFET LFC schemes are compared in Figs. 21 (a) and (b). The transmission amounts of the ACE signal for the studied system under different control schemes are listed in Table V. The fuzzy gains α_3 of area 3 of the studied system are displayed in Fig. 22. $(CF)_1$ and the aggregative 1-minute average CF_{av} of area 3 of the studied system are shown in Figs.23 (a) and (b), respectively. Additionally, the 10-minute averages of the ACE from the three areas are calculated and compared with the constants L_{10-i} with $i = 1, 2, 3$ in Figs. 24 (a), (b) and (c). The responses of these results of areas 1 and 2 are similar and omitted here due to space limitations.

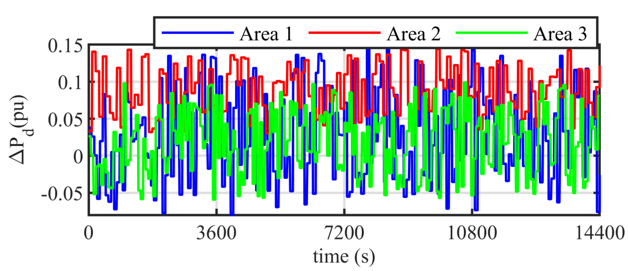

Fig. 19. Random changes of load of three areas.

TABLE V
AMOUNTS OF SIGNAL TRANSMISSION IN DIFFERENT CONTROL SCHEMES

Schemes	CPSFET	CPSET	AET	ET	TT
Area 1	218	487	841	860	3600
Area 2	282	426	841	845	3600
Area 3	144	551	1125	1118	3600

Figs. 21 (a) and 22 show that the proposed scheme can adaptively change the threshold parameters and fuzzy gains along with the inputs of CF_{av-3}. Under the action of these fuzzy gains, the control inputs of the proposed CPSFET LFC scheme are obviously reduced compared with those of other non-fuzzy-based LFC schemes, as shown in Figs. 20 (a). Although the proposed scheme does not generate the maximum threshold parameter in comparison with the other schemes according to Fig. 21 (a), it can be found from Fig. 21 (b) and Table V that the scheme further reduces unnecessary transmission of the control signal. In detail, by applying equation (27), compared with the traditional TT LFC scheme, the amounts of signal transmission in the three areas are found to be reduced by 93.94%, 92.17% and 96%, while they are reduced by 55.24%, 33.80% and 73.87% compared with the optimal CPSET LFC scheme among the existing control schemes. Meanwhile, the responses of the system frequency and the ACE of area 3 are essentially similar without drastic changes, as shown in Figs. 20 (b).

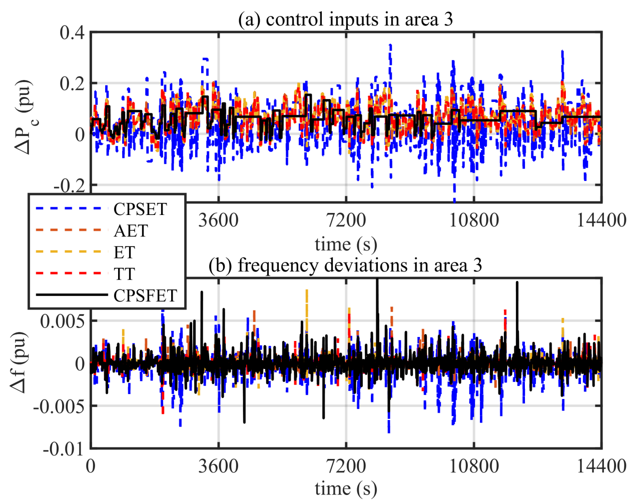

Fig. 20. Control inputs and frequency deviations of area 3.

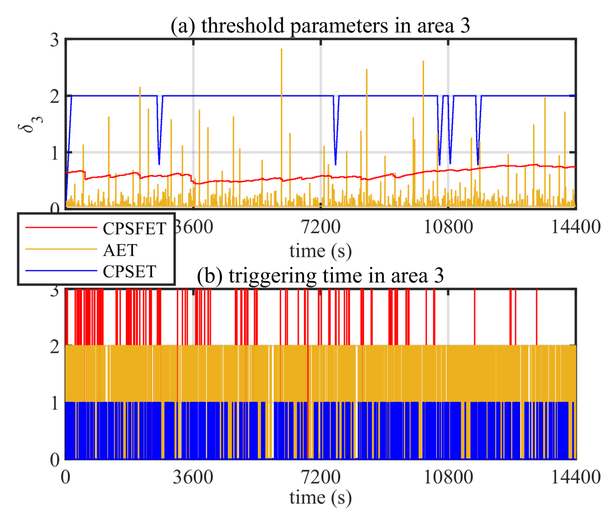

Fig. 21. Threshold parameters and triggering time of area 3.

Considering Fig. 23, it can be seen that the proposed scheme can make the $(CF_3)_1$ of the system lower or higher than 1 so that the aggregative 1-minute average CF_{av-3} can be maintained within a certain range and just meet the CPS1 requirement. In contrast, in the other LFC schemes, most of the $(CF_3)_1$ values are less than 1, which makes the aggregative 1-minute average CF_{av} decrease all the time, thus resulting in the CPS1 requirement being overly satisfied. In addition, it can be observed from Fig. 24 that the 10-minute averages of the ACE in every control area crosses the upper bounds L_{10-i} only once within four hours. After a simple calculation, the CPS2 within four hours in every control area is $(CPS2)_{4-hour} = 100(1-1/24) = 95.83\% < 90\%$, meeting the CPS2 requirement.

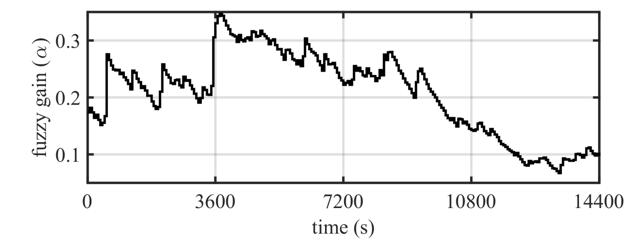

Fig. 22. Fuzzy gains in area 3.

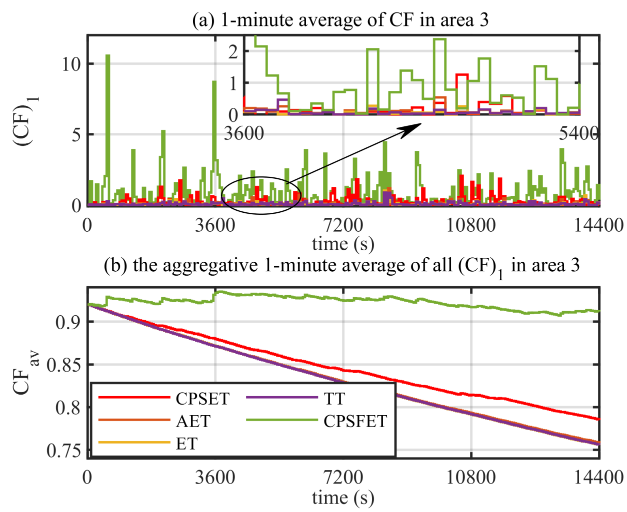

Fig. 23. CF_1 and CF_{ac} in area 3.

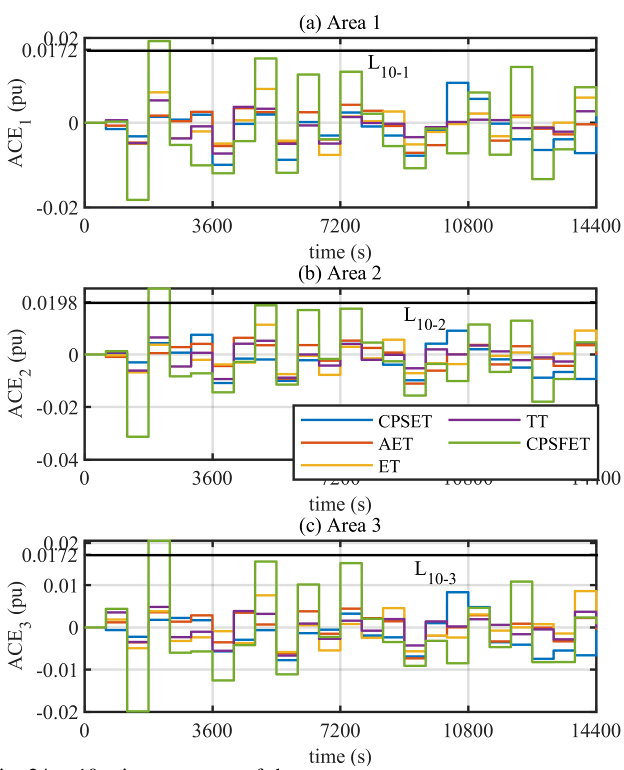

Fig. 24. 10-minute average of three areas.

From the test results of the LFC scheme for the IEEE 39-bus test system, it can be concluded that the proposed CPSFET LFC scheme is effective and superior. The proposed CPSFET LFC can meet the requirements of CPS1 and CPS2. Moreover, compared with other non-fuzzy-based LFC schemes, the proposed CPSFET LFC scheme can both reduce the wear and tear on the generating unit equipment and further lower the use of communication bandwidth.

V. Conclusion

In this paper, the CPS-based fuzzy event-triggered scheme has been proposed for LFC of power systems to solve the problems of wear and tear on the generating unit equipment and limited communication bandwidth. The proposed control scheme consists of the CPS-based fuzzy control system and the function expression-based adjustable event-triggered communication scheme. The fuzzy control system is used to reduce the wear and tear by following the compliance factor of CPS1, while the adjustable event-triggered scheme is employed to save more communication bandwidth. Case studies based on the simple one-area power system and the complex IEEE 39-bus benchmark test system have been undertaken to verify the effectiveness of the proposed scheme. In addition, to illustrate the advantages of the proposed scheme, the simulation test results obtained under the proposed scheme have been compared with the results from the existing non-fuzzy-based LFC schemes, including the CPSET, AET, ET and TT LFC schemes. The results demonstrate that the proposed control scheme reduces wear and tear and saves more communication network bandwidth compared to the other control schemes while ensuring the requirements of CPS1 and CPS2.

The fuzzy-based active disturbance rejection control scheme proposed in Ref. [19] can actively suppress disturbance changes. In LFC, the load can be treated as a system disturbance, so if the fuzzy-based active disturbance rejection could be combined with the proposed control scheme to actively eliminate the impact of the load, then it will be able to further reduce signal transmission and the wear and tear. This is considered to be a future research direction.

Appendix

Proof of Theorem 1

To complete the proof of Theorem 1, the following lemma is first introduced.

Lemma 1: (Wirtinger-based integral inequality [38]) Let x be a differentiable signal in $[a,b] \to \mathbb{R}^n$; for positive definite symmetric matrix $H \in \mathbb{R}^{n\times n}$, the following inequality holds:

$$-\int_a^b \dot{x}^T(s)H\dot{x}(s)ds \le \frac{1}{b-a}\varpi^T\Gamma^T \begin{bmatrix} H & 0 \\ 0 & 3H \end{bmatrix} \Gamma\varpi \quad (28)$$

where

$$\varpi = \begin{bmatrix} x^T(b) & x^T(a) & \frac{1}{b-a}\int_a^b x^T(s)ds \end{bmatrix}^T$$
$$\Gamma = \begin{bmatrix} I_n & -I_n & 0_{n\times n} \\ I_n & I_n & -2I_n \end{bmatrix}.$$

To simplify the notation, $\rho = f_d + l$ is introduced. The discrete-time model of system (15) with zero disturbance is obtained by integrating the differential equation (15) over the interval $[t_\rho, t_\rho + \eta]$ for any η in $[0, \bar{T}_\rho]$ with $\bar{T}_\rho \in [\bar{h}_1, \bar{h}_2]$,

$$x_i(t_\rho+\eta)=\tilde{A}_i(\eta)x_i(t_\rho)+\tilde{A}_{id}(\eta)(x_{ei}(s_\rho)-x_i(t-\varsigma(t)))$$
$$\tilde{A}_i(\eta)=e^{A_i\eta},\quad \tilde{A}_{id}(\eta)=\int_0^\eta e^{A_i(\eta-\theta)}d\theta B_iK_iC_i$$

Then, for all integers ρ, define the function $\chi_\rho:[0,\bar{T}_\rho]\times[-\tau(s_\rho),0]\longrightarrow\mathbb{R}^n$ such that for all η in $[0,\bar{T}_\rho]$ and all ϵ in $[-\tau(s_\rho),0]$, $\chi_\rho(\eta,\epsilon)=x_i(t_\rho+\eta+\epsilon)$. Then, choose a Lyapunov-Krasovskii functional as follows

$$V(\chi_\rho)=V_1(\chi_\rho)+V_2(\eta,\chi_\rho) \tag{29}$$

where

$$\begin{aligned}V_1(\chi_\rho)=&\xi_1{}^TP\xi_1+\int_{-\tau(s_\rho)}^0\chi_\rho^T(\eta,s)M\chi_\rho(\eta,s)ds\\&+\int_{-\tau(s_\rho)}^0\dot{\chi}_\rho^T(\eta,s)N\dot{\chi}_\rho(\eta,s)ds\\&+\int_{-\tau(s_\rho)}^0\int_\lambda^0\dot{\chi}_\rho^T(\eta,s)H\dot{\chi}_\rho(\eta,s)dsd\lambda\\V_2(\eta,\chi_\rho)=&Sym\left(\xi_2^T\left(Q_1\xi_3+Q_2\xi_4\right)\right)+\left(\bar{T}_\rho-\eta\right)\eta\xi_4^TZ\xi_4\\&+Sym\left(\left(z^T(\eta)-z^T(0)\right)X\left(z(\eta)-z\left(\bar{T}_\rho\right)\right)\right)\\&+\left(\bar{T}_\rho-\eta\right)\int_0^\eta\dot{z}^T(s)R_1\dot{z}(s)ds\\&-\eta\int_\eta^{\bar{T}_\rho}\dot{z}^T(s)R_2\dot{z}(s)ds\end{aligned}$$

with

$$z(\eta)=[\chi_\rho^T(\eta,0)\chi_\rho^T(\eta,-\tau(s_\rho))]^T,\xi_1=[z^T(\eta)\int_{-\tau(s_\rho)}^0\chi_\rho^T(\eta,s)ds]^T$$
$$\xi_2=[\left(\bar{T}_\rho-\eta\right)\left(z^T(\eta)-z^T(0)\right)\ \ \eta\left(z^T(\eta)-z^T\left(\bar{T}_\rho\right)\right)]^T$$
$$\xi_3=[z^T(\eta)-z^T(0)\ \ z^T(\eta)-z^T\left(\bar{T}_\rho\right)]^T,\xi_4=[z^T(0)\ \ z^T\left(\bar{T}_\rho\right)]^T$$

$$\varphi=[z^T(\eta)\ \ \dot{\chi}_\rho^T(\eta,-\tau(s_\rho))\ \ z^T(0)\ \ z^T(\bar{T}_\rho)\ \ \frac{1}{\tau_M}\int_{-\tau(s_\rho)}^0\chi_\rho^T(\eta,s)ds\ \ x_e^T(s_{f_d+j})]^T.$$

Note that $V_2(\eta,\chi_\rho)$ is a looped functional satisfies $V_2(0,\chi_\rho)=V_2(\bar{T}_\rho,\chi_\rho)=0$. Based on theorem 1 in [37], to guarantee the stability of system (15), the objective is to ensure that the variation in $V_1(\chi_\rho)$ between two successive sampling instants is strictly negative. Therefore, the remainder of the proof ensures that $\dot{V}(\chi_\rho)=\frac{d}{d\eta}\left[V_1\left(\chi_\rho(\eta,\cdot)\right)+V_2\left(\eta,\chi_\rho(\cdot,\cdot)\right)\right]<0$. One can obtain

$$\begin{aligned}\dot{V}(\chi_\rho)\leq&\varphi^T(e_1^TMe_1-e_2^TMe_2+E_0^TNE_0-e_3^TNe_3+\tau_ME_0^THE_0\\&+Sym\{\Pi_1^TP\Pi_{21}+\Pi_{71}^TQ_1\Pi_{72}+\Pi_{71}^TQ_2\Pi_8\\&+\Pi_2^TX(\Pi_4-\Pi_6)+(\Pi_4-\Pi_5)^TX\Pi_2\})\varphi\\&+(\bar{T}_\rho-\eta)\varphi^T\Theta_2\varphi+\eta\varphi^T\Theta_3\varphi-\int_{-\tau(s_\rho)}^0\dot{\chi}_\rho^T(\eta,s)H\dot{\chi}_\rho(\eta,s)ds\\&-\int_0^\eta\dot{z}^T(s)R_1\dot{z}(s)ds-\int_\eta^{\bar{T}_\rho}\dot{z}^T(s)R_2\dot{z}(s)ds\end{aligned}$$

The first integral term of $\dot{V}(\chi_\rho)$ can be bounded by applying Lemma 1:

$$\begin{aligned}-\int_{-\tau(s_\rho)}^0\dot{\chi}_\rho^T(\eta,s)H\dot{\chi}_\rho(\eta,s)ds\leq&-\frac{1}{\tau(s_\rho)}\varphi^T\Pi_3^T\begin{bmatrix}H&0\\0&3H\end{bmatrix}\Pi_3\varphi\\\leq&-\frac{1}{\tau_M}\varphi^T\Pi_3^T\begin{bmatrix}H&0\\0&3H\end{bmatrix}\Pi_3\varphi\end{aligned} \tag{30}$$

Then, any matrices U_1 and U_2 satisfy the following zero-equations based on the free-weight-matrix technique

$$0=2\varphi^TU_1\left(z(0)-z(\eta)+\int_0^\eta\dot{z}(s)ds\right) \tag{31}$$
$$0=2\varphi^TU_2\left(z(\eta)-z(\bar{T}_\rho)+\int_\eta^{\bar{T}_\rho}\dot{z}(s)ds\right). \tag{32}$$

According to ET condition (9) $\partial_2(j)\leq0$, one can obtain the following inequality:

$$\Upsilon=\delta_ix_i^T\left(s_{f_d}\right)\Omega_ix_i\left(s_{f_d}\right)-x_{ei}^T\left(s_{f_d+j}\right)\Omega_ix_{ei}\left(s_{f_d+j}\right)\geq0 \tag{33}$$

That is:

$$\Upsilon=\delta_i(e_5-e_9)^T\Omega_i(e_5-e_9)-e_9^T\Omega_ie_9\geq0 \tag{34}$$

Next, add zero-equations (31) and (32) and non-negative matrix Υ into the derivative, and replace the integral term of H by inequality (30) in the derivative. This yields

$$\begin{aligned}\dot{V}(\chi_\rho)\leq&\varphi^T(e_1^TMe_1-e_2^TMe_2+E_0^TNE_0-e_3^TNe_3+\tau_ME_0^THE_0\\&+Sym\{\Pi_1^TP\Pi_{21}+\Pi_{71}^TQ_1\Pi_{72}+\Pi_{71}^TQ_2\Pi_8\\&+\Pi_2^TX(\Pi_4-\Pi_6)+(\Pi_4-\Pi_5)^TX\Pi_2\}\\&+\delta_i(e_5-e_9)^T\Omega_i(e_5-e_9)-e_9^T\Omega_ie_9)\varphi\\&-\frac{1}{\tau_M}\varphi^T\Pi_3^T\begin{bmatrix}H&0\\0&3H\end{bmatrix}\Pi_3\varphi\\&-2\varphi^TU_1(\Pi_4-\Pi_5)\varphi+2\varphi^TU_2(\Pi_4-\Pi_6)\varphi\\&+2\varphi^TU_1\int_0^\eta\dot{z}(s)ds+2\varphi^TU_2\int_\eta^{\bar{T}_\rho}\dot{z}(s)ds\\&+(\bar{T}_\rho-\eta)\varphi^T\Theta_2\varphi+\eta\varphi^T\Theta_3\varphi\\&-\int_0^\eta\dot{z}^T(s)R_1\dot{z}(s)ds-\int_\eta^{\bar{T}_\rho}\dot{z}^T(s)R_2\dot{z}(s)ds\end{aligned}$$

Then the derivative can be rewritten as follows:

$$\begin{aligned}\dot{V}(\chi_\rho)\leq&\frac{(\bar{T}_\rho-\eta)+\eta}{\bar{T}_\rho}\varphi^T\Theta_1\varphi+\frac{\bar{T}_\rho-\eta}{\bar{T}_\rho}\varphi^T\Theta_2\varphi+\frac{\eta}{\bar{T}_\rho}\varphi^T\Theta_3\varphi\\&+\frac{1}{\bar{T}_\rho}\int_0^\eta2\varphi^TU_1\dot{z}(s)ds+\frac{1}{\bar{T}_\rho}\int_\eta^{\bar{T}_\rho}2\varphi^TU_2\dot{z}(s)ds\\&-\frac{1}{\bar{T}_\rho}\int_0^\eta\dot{z}^T(s)\bar{T}_\rho R_1\dot{z}(s)ds-\frac{1}{\bar{T}_\rho}\int_\eta^{\bar{T}_\rho}\dot{z}^T(s)\bar{T}_\rho R_2\dot{z}(s)ds\\=&\frac{1}{\bar{T}_\rho}\int_\eta^{\bar{T}_\rho}\begin{bmatrix}\varphi\\\dot{z}(s)\end{bmatrix}^T\Xi_1\begin{bmatrix}\varphi\\\dot{z}(s)\end{bmatrix}ds+\frac{1}{\bar{T}_\rho}\int_0^\eta\begin{bmatrix}\varphi\\\dot{z}(s)\end{bmatrix}^T\Xi_2\begin{bmatrix}\varphi\\\dot{z}(s)\end{bmatrix}ds\end{aligned} \tag{35}$$

Considering that the inner matrix on the right side of (35) is linear and therefore convex with respect to $\bar{T}_\rho\in[\bar{h}_1,\bar{h}_2]$, the right-hand of (35) is negative definite if $\Xi_1<0$ and $\Xi_2<0$. This completes the proof.

References

[1] L. Jiang, W. Yao, Q. H. Wu, et al., "Delay-dependent stability for load frequency control with constant and time-varying delays," *IEEE Trans. Power Syst.*, vol. 27, no. 2, pp. 932–941, May 2012.

[2] H. Bevrani. *Robust Power System Frequency Control*. New York: Springer, 2014.

[3] L. Jin, C. K. Zhang, Y. He, et al., "Delay-dependent stability analysis of multi-area load frequency control with enhanced accuracy and computation efficiency," *IEEE Trans. Power Syst.*, vol. 34, no. 5, pp. 3687–3696, Sept. 2019.

[4] C. Yang, W. Yao, J. Fang, et al., “Dynamic event-triggered robust secondary frequency control for islanded AC microgrid,” *Appl. Energy*, vol. 242, pp. 821–836, May 2019.
[5] C. K. Zhang, L. Jiang, Q. H. Wu, et al., “Delay-dependent robust load frequency control for time delay power systems,” *IEEE Trans. Power Syst.*, vol. 28, no. 3, pp. 2192–2201, Aug. 2013.
[6] A. Pappachen, A. P. Fathima, “Critical research areas on load frequency control issues in a deregulated power system: A state-of-the-art-of-review,” *Renew. Sust. Energ. Rev.*, vol. 72, pp. 163–177, May 2017.
[7] A. Feliachi, D. Rerkpreedapong, “NERC compliant load frequency control design using fuzzy rules,” *Electr. Power Syst. Res.*, vol. 73, no. 2, pp. 101–106, Feb. 2005.
[8] H. Shayeghi, A. Jalili, H. A. Shayanfar, “Robust modified GA based multi-stage fuzzy LFC,” *Energy Convers. Manage.*, vol. 48, no. 5, pp. 1656–1670, May 2007.
[9] J. Liu, W. Yao, J. Y. Wen. et al., “Impact of power grid strength and pll parameters on stability of grid-connected DFIG wind farm,” *IEEE Trans. Sustain. Energy*, vol. 11, no. 1, pp. 545–557, Jan. 2020.
[10] L. Dong, Y. Tang, H. He, et al., “An event-triggered approach for load frequency control with supplementary ADP,” *IEEE Trans. Power Syst.*, vol. 32, no. 1, pp. 581–589, Jan. 2017.
[11] Z. Shi, W. Yao, Z. Li, et al., “Artificial intelligence techniques for stability analysis and control in smart grids: Methodologies, applications, challenges and future directions,” *Appl. Energy*, vol. 278, pp. 115733, Nov. 2020.
[12] V. C. Gungo, D. Sahin, T. Kocak, et al., “Smart grid technologies: Communication technologies and standards,” *IEEE Trans. Ind. Inf.*, vol. 7, no. 4, pp. 529–539, Nov. 2011.
[13] C. Li, X. Yu, W. Yu, et al., “Distributed event-triggered scheme for economic dispatch in smart grids,” *IEEE Trans. Ind. Inf.*, vol. 12, no. 5, pp. 1775–1785, Oct. 2016.
[14] L. Wang, Z. Wang, Q. Han, et al., “Synchronization control for a class of discrete-time dynamical networks with packet dropouts: A coding-decoding-based approach,” *IEEE Trans. Cybern.*, vol. 48, no. 8, pp. 2437–2448, Aug. 2018.
[15] Y. Wang, I. R. Pordanjani, W. Xu, “An event-driven demand response scheme for power system security enhancement,” *IEEE Trans. Smart Grid*, vol. 2, no. 1, pp. 23–29, March 2011.
[16] G. Gross, J. W. Lee, “Analysis of load frequency control performance assessment criteria,” *IEEE Trans. Power Syst.*, vol. 16, no. 3, pp. 520–525, Aug. 2011.
[17] T. Haidegger, L. Kovcs, R. E. Precup, et al., “Simulation and control for telerobots in space medicine,”. *Acta Astronaut.*, vol. 81, no. 1, pp. 390–402, Dec. 2012.
[18] A. Csapo, P Baranyi, “The spiral discovery method: An interpretable tuning model for CogInfoCom channels,” *J. Adv. Comput. Intell. Intell. Inf.*, 2012, vol. 16, no. 2, pp. 358–367, Nov. 2012.
[19] R. C. Roman, R. E. Precup, E. M. Petriu, “Hybrid data-driven fuzzy active disturbance rejection control for tower crane systems,” *Eur. J. Control*, vol. 58, pp. 373–387, March 2021.
[20] S. K. Yee, J. V. Milanovic, “Fuzzy logic controller for decentralized stabilization of multimachine power systems,” *IEEE Trans. Fuzzy Syst.*, vol. 16, no. 4, pp. 971–981. Aug. 2008.
[21] S. Falahati, S. A. Taher, M. Shahidehpour, “Grid secondary frequency control by optimized fuzzy control of electric vehicles,” *IEEE Trans. Smart Grid*, vol. 9, no. 6, pp. 5613–5621, Nov. 2018.
[22] T. Zhang, G. Feng, “Rapid load following of an SOFC power system via stable fuzzy predictive tracking controller,” *IEEE Trans. Fuzzy Syst.*, vol. 17, no. 2, pp. 357–371, April 2009.
[23] K. H. Chua, Y. S. Lim, S. Morris, “A novel fuzzy control algorithm for reducing the peak demands using energy storage system,” *Energy*, vol. 122, pp. 265–273, March 2017.
[24] H. Ma, H. Li, H. Liang, et al., “Adaptive fuzzy event-triggered control for stochastic nonlinear systems with full state constraints and actuator faults,” *IEEE Trans. Fuzzy Syst.*, vol. 27, no. 11, pp. 2242–2254, Nov. 2019.
[25] S. Li, C. K. Ahn, M. Chadli, et al., “Sampled-data adaptive fuzzy control of switched large-scale nonlinear delay systems,” *IEEE Trans. Fuzzy Syst.*, early access, 2021. Doi: 10.1109/TFUZZ.2021.3052094.
[26] A. Pappachen, A. P. Fathima, “NERCs control performance standards based load frequency controller for a multi area deregulated power system with ANFIS approach,” *Ain Shams Eng. J.*, vol. 9, no. 4, pp. 2399–2414, Dec. 2018.
[27] R. Belkacemi, A. N. Rimal, “A novel NERC compliant automatic generation control in multi-area power systems in the presence of renewable-energy resources,” *Electr. Eng.*, vol. 99, no. 3, pp. 931–941, Oct. 2016.
[28] Z. Fei, S. Shi, C. K. Ahn, et al., “Finite-time control for switched t-s fuzzy systems via dynamic event-triggered mechanism,” *IEEE Trans. Fuzzy Syst.*, early access, 2020. Doi: 10.1109/TFUZZ.2020.3029292.
[29] Z. Wang, Q. Liu, D. Wang, et al., “Event-triggered tracking control of heterogeneous multiagent systems based on two kinds of observers with asymmetric delay.” *Int. J. Robust Nonlinear Control*, vol. 29, no. 10, pp. 2862–2876, March, 2019.
[30] S. Wen, X. Yu, Z. Zeng, et al., “Event-triggering load frequency control for multi-area power systems with communication delays,” *IEEE Trans. Ind. Electron.*, vol. 63, no. 2, pp. 1308–1317, Feb. 2016.
[31] C. Peng, J. Zhang, H. Yan, “Adaptive event-triggering H_∞ load frequency control for network-based power systems,” *IEEE Trans. Ind. Electron.*, vol. 65, no. 2, pp. 1685–1694, Feb. 2018.
[32] H. Zhang, S. Su, Y. Y. Zhao, et al., “Networked load frequency control of multi-area uncertain power systems via adaptive event-triggered communication scheme,” *J. Franklin Inst.*, vol. 356, no. 16, pp. 9600–9626, Nov. 2019.
[33] S. Saxena, E. Fridman, “Event-triggered load frequency control via switching approach,” *IEEE Trans. Power Syst.*, vol. 35, no. 6, pp. 4484–4494, Nov. 2020.
[34] X. C. Shangguan, Y. He, C. K. Zhang, et al. “Control performance standards-oriented event-triggered load frequency control for power systems under limited communication bandwidth,” *IEEE Trans. Control Syst. Technol.*, early access, 2021. Doi: 10.1109/TCST.2021.3070861.
[35] H. F. Illian, “Frequency control performance measurement and requirements,” *Energy Mark Inc.*, Dec. 2010.
[36] I. Hiskens, “IEEE PES task force on benchmark systems for stability controls,” *Tech. Rep. 39–bus system (New England reduced model)*, 2013.
[37] A. Seuret, “A novel stability analysis of linear systems under asynchronous samplings,” *Automatica*, vol. 48, no. 1, pp.177–182, Jan. 2012.
[38] A. Seuret, F. Gouaisbaut, “Wirtinger-based integral inequality: Application to time-delay systems,” *Automatica*, vol. 49, no. 9, pp. 2860–2866, Sep. 2013.
[39] X. C. Shangguan, Y. He, C. K. Zhang, et al., “Switching system-based load frequency control for multi-area power system resilient to denial-of-service attacks,” *Control Eng. Pract.*, vol 107, pp. 104678, Feb. 2021.
[40] X. C. Shangguan, Y. He, C. K. Zhang, et al., “Robust load frequency control for power system considering transmission delay and sampling period,” *IEEE Trans. Ind. Inf.*, vol. 17, no.8, pp. 5292–5303, Aug. 2021.
[41] L. Cao, H. Li, N. Wang, et al., “Observer-based event-triggered adaptive decentralized fuzzy control for nonlinear large-scale systems,” *IEEE Trans. Fuzzy Syst.*, vol. 27, no. 6, pp. 1201–1214, June 2019.
[42] C. Peng, J. Zhang, “Delay-distribution-dependent load frequency control of power systems with probabilistic interval delays,” *IEEE Trans. Power Syst.*, vol. 31, no. 4, pp. 3309–3317, July 2015.